Title
Molecular height measurement by cell surface optical profilometry (CSOP)

Journal
Proceedings of the National Academy of Sciences of the United States of America, 117(25)

ISSN
0027-8424

Authors
Son, Sungmin
Takatori, Sho C
Belardi, Brian
et al.

Publication Date
2020-06-23

DOI
10.1073/pnas.1922626117

Peer reviewed

Molecular height measurement by cell surface optical profilometry (CSOP)

Sungmin Son[a], Sho C. Takatori[a], Brian Belardi[a], Marija Podolski[a], Matthew H. Bakalar[a,1], and Daniel A. Fletcher[a,b,c,2]

[a]Department of Bioengineering and Biophysics Program, University of California, Berkeley, CA 94720; [b]Division of Biological Systems and Engineering, Lawrence Berkeley National Laboratory, Berkeley, CA 94720; and [c]Chan Zuckerberg Biohub, San Francisco, CA 94158

Edited by Jennifer Lippincott-Schwartz, Janelia Farm Research Campus, Ashburn, VA, and approved May 4, 2020 (received for review December 27, 2019)

The physical dimensions of proteins and glycans on cell surfaces can critically affect cell function, for example, by preventing close contact between cells and limiting receptor accessibility. However, high-resolution measurements of molecular heights on native cell membranes have been difficult to obtain. Here we present a simple and rapid method that achieves nanometer height resolution by localizing fluorophores at the tip and base of cell surface molecules and determining their separation by radially averaging across many molecules. We use this method, which we call cell surface optical profilometry (CSOP), to quantify the height of key multidomain proteins on a model cell, as well as to capture average protein and glycan heights on native cell membranes. We show that average height of a protein is significantly smaller than its contour length, due to thermally driven bending and rotation on the membrane, and that height strongly depends on local surface and solution conditions. We find that average height increases with cell surface molecular crowding but decreases with solution crowding by solutes, both of which we confirm with molecular dynamics simulations. We also use experiments and simulations to determine the height of an epitope, based on the location of an antibody, which allows CSOP to profile various proteins and glycans on a native cell surface using antibodies and lectins. This versatile method for profiling cell surfaces has the potential to advance understanding of the molecular landscape of cells and the role of the molecular landscape in cell function.

plasma membrane | superresolution microscopy | cell surface topography | CD45 | antibodies

The surface of cells contains a dense and diverse population of molecules including proteins, glycosylated proteins, and glycolipids that extend above the plasma membrane. The average height of these proteins and glycans, which reflects their most common configurations, depends on structure as well as flexibility and local interactions. The size of individual folded domains can be obtained from crystal structures, which provide good estimates for the height of membrane proteins with single ectodomains, such as the 5-nm-tall "marker of self" CD47 (1). However, membrane proteins with ectodomains larger than a single IgG domain, which constitute ∼51% of the human surface proteome (2) (see *Materials and Methods*), have heights that are not simply the sum of their individual domains, due to domain organization, flexibility between domains, and thermally driven fluctuations that reduce average extension from the surface. For example, the average height of the seven-domain CEACAM5 adhesion molecule will be smaller than its maximum fully extended height of 29.7 nm obtained by summing domain sizes. This uncertainty in multidomain protein height is compounded by contributions from unstructured domains and glycosylation that make estimates based on sequence and structure alone imprecise. For the protein tyrosine phosphatase CD45, which has four structured domains, for example, the average height of its isoforms will be variable depending on an N-terminal unstructured domain, and multiple glycosylation sites. Moreover, since cell surface densities are ∼20,000 molecules per square micrometer (3), which corresponds to an average spacing of ∼7 nm between molecules, the average heights of membrane proteins and glycans may be further altered by crowding.

Recent studies have revealed a critical role for cell surface molecular landscapes in cell function. In the immune system, size-dependent segregation of proteins has been shown to modulate T cell activation by antigen-presenting cells (4–7), broaden mast cell and basophil reactivity (8), and promote antibody-dependent phagocytosis by macrophages (9), where an antigen height difference of as little as 5 nm can significantly alter phagocytic efficiency. In cancer, increased glycocalyx height can drive integrin overactivation and promote tumor cell survival (10) and metastasis (11). In simulations of integrin binding, an increase in the glycocalyx height of 4 nm was predicted to reduce the fraction of bound integrin by an order of magnitude (12), while simulations of fluctuating membranes predicted that nanometer-scale height displacements of proteins can significantly alter ligand–receptor binding kinetics (13).

Despite the importance of the cell surface molecular landscapes in diverse cell functions, current techniques are not able to provide rapid and specific nanometer-scale measurements of cell surface molecular heights on native cell membranes. Transmission electron microscopy has been used extensively to image the glycocalyx of cells (14), although it is limited in its molecular specificity and requires lengthy sample preparations known to distort the glycocalyx

Significance

The heights of membrane proteins, glycoproteins, and glycolipids play a critical role in multiple cellular activities, including cancer progression and immune cell signaling. However, methods for accurately quantifying molecular heights, which can range from 1 nm to more than 100 nm, are needed. To address this need, we use single-molecule localization in one dimension averaged across multiple molecules to measure height with ∼1-nm resolution. The method, which we call cell surface optical profilometry (CSOP), can accurately quantify the average height of multidomain proteins, detect changes in height due to crowding, and report average protein and glycan heights on native cell surfaces. CSOP provides a new tool for measuring and investigating the functional roles of cell surface molecular landscapes.

Author contributions: S.S., M.H.B., and D.A.F. conceived of the study; S.S., B.B., M.P., and D.A.F. designed research; S.S. and M.P. performed research; S.S. and M.H.B. analyzed data; S.C.T. performed molecular dynamics simulations; B.B. and D.A.F. interpreted the data; D.A.F. supervised the study; and S.S., S.C.T., and D.A.F. wrote the paper.

The authors declare no competing interest.

This article is a PNAS Direct Submission.

Data deposition: Supplementary software is available in Github (https://github.com/smson-ucb/CSOP).

[1]Present address: Broad Institute of MIT and Harvard, Cambridge, MA 02142.

[2]To whom correspondence may be addressed. Email: fletch@berkeley.edu.

This article contains supporting information online at https://www.pnas.org/lookup/suppl/doi:10.1073/pnas.1922626117/-/DCSupplemental.

First published June 8, 2020.

(15). Several optical-based methods have been developed to quantify distances, such as scanning-angle interference microscopy (16) and fluorescence interference contrast microscopy (17, 18), but these methods require close contact of cells with a surface that can affect the natural extension of cell surface molecules. Fluorescence resonance energy transfer (FRET) can be used to quantify distances between two fluorophores on a single molecule (19), although FRET-based approaches lack the dynamic range needed to capture the full range of cell surface molecular heights, which can extend 300 nm above the membrane for some glycosylated proteins (14). Three-dimensional (3D) superresolution imaging techniques such as interferometric PhotoActivated Localization Microscopy (iPALM) (20), point spread function engineering (21), and multiplane imaging (22, 23) have been successfully used to image protein organization in integrin- (24) and cadherin-based cell adhesion (25), as well as to quantify the average thickness of the glycocalyx of cancer cells (26). However, these techniques often require a cell to be fixed to achieve high resolution, which can disrupt the native configurations of cell surface molecules, and typically do not exceed single-molecule localization accuracy of ∼10-nm resolution, unless highly specialized (27, 28). Since cell surface molecular height differences of just a few nanometers can significantly change cell function, a simple characterization method with resolution significantly better than 10 nm is needed.

Here we present a method for quantifying cell surface molecular height with ∼1-nm resolution that can be used to rapidly profile proteins and glycans on unfixed membrane surfaces, including native cell membranes. This method, which we call cell surface optical profilometry (CSOP), uses radial averaging of thousands of fluorescently labeled molecules to achieve high localization accuracy and nanometer-scale height resolution (Fig. 1*A*). We validate CSOP by measuring the average end-to-end distance of tethered double-stranded DNA (dsDNA) and by quantifying the thickness of bilayer membranes formed from different lipid compositions. We then use CSOP to measure the height and determine the flexibility of native and synthetic multidomain proteins, and we investigate how crowding and solution conditions can alter height. Molecular dynamics (MD) simulations used to corroborate CSOP measurements reveal that certain dynamical/physical features of cell surface proteins may be understood in the classical framework of semiflexible polymers. We show that CSOP can also be used to localize the protein domain targeted by an antibody and to determine the average heights of individual molecular species as well as the entire cell surface proteome and glycome on native cell membranes. This simple, rapid, and versatile method for height measurement can provide insight into the role played by cell surface molecular landscapes in diverse cellular processes.

Results

The Principle of CSOP. CSOP draws inspiration from recent superresolution microscopy methods that are based on precise localization of individual flourophores (30). However, rather than localizing in three dimensions, CSOP achieves nanometer-scale resolution of cell surface molecules in one dimension, height, by foregoing positional information in lateral dimensions. Height is determined using two fluorophores, one at the tip of the cell surface molecule to be measured and the other on the membrane in which the molecule is anchored. The fluorescently labeled molecules are arranged in a spherical geometry, such as on a glass bead, giant vesicle, or swollen cell, so that multiple molecules oriented axisymmetrically can be averaged to obtain a measurement of fluorophore radius with high precision. Height is then quantified as the difference in radii of the two fluorophores.

This approach overcomes the typical ∼10-nm resolution limit of single-molecule localization by increasing the number of fluorophores used in the radius localization by orders of magnitude (Fig. 1*B*). Tens to hundreds of thousands of fluorophores indicating the same position in the radial coordinate enhance the radial intensity profile above background noise, enabling high-resolution determination of average separation between fluorophores. Typical stochastic optical reconstruction microscopy (STORM) imaging collects 3,000 photons from a single fluorophore per exposure, which corresponds to a ratio of peak signal to photon shot noise of 20. In practice, this signal-to-noise ratio (SNR) = 20 enables localization of the fluorophore with 8-nm precision, after careful removal of drift (31). For a measurement of fluorescently labeled proteins bound to the surface of a bead (Fig. 1 *A* and *B*), CSOP achieves 0.65-nm precision for the same SNR by radially averaging, in this case, ∼550 labeled proteins per square micrometer from which we collect ∼100 photons per fluorophore (Fig. 1*B* and *SI Appendix*, Table S1). If we increase the density of labeled proteins to 1,000 per square micrometer but continue to collect the same number of photons per fluorophore, this localization precision is increased to 0.5 nm, although this is below the predicted precision of 0.3 nm that should be theoretically possible for a shot noise limited measurement (Fig. 1*C* and *SI Appendix*, Table S1). For typical densities of labeled molecules on cell surfaces, a height resolution of ∼1 nm is readily obtained.

Notably, this approach to cell surface molecular height measurement enables simple multiplexing of height measurements by labeling different cell surface molecules on the same membrane with different fluorophores, making it possible for CSOP to simultaneously profile multiple proteins and glycans using standard multichannel fluorescence microscopy.

Validation of Molecular Height Measurements with CSOP. We set up CSOP on a standard spinning disk confocal microscope with a sCMOS camera and a high-numerical aperture (NA) objective (Yokogawa CSU-X1, Andor Zyla 4.2, 100×/1.49 Apo). To demonstrate height measurements with CSOP, we used lipid-coated glass beads with purified molecules attached to the outer leaflet of the membrane, with Alexa 488 localizing the membrane distal end of the molecule and Alexa 555 localizing the membrane surface. We corrected for chromatic aberrations, which can introduce errors into CSOP measurements (*SI Appendix*, Fig. S1) (32), by implementing a calibration procedure before imaging the sample (*SI Appendix*, Fig. S2 and *SI Materials and Methods*). We also addressed polarization effects associated with fluorescent labels that insert into membranes by using an alternate membrane-bound label (*SI Appendix*, Fig. S3 and *SI Materials and Methods*) (33).

As a validation of CSOP's height measurement capabilities, we measured the end-to-end distance of dsDNA tethered to a surface. We quantified the average separation between a bilayer membrane and the fluorescently labeled end of dsDNA ranging from 18 to 103 base pairs (bp) (*SI Appendix*, Table S2). We found that the CSOP height measurements, <h>, agree well with predictions based on previously measured DNA end-to-end lengths and a persistence length of 50 nm (34) (Fig. 1*D* and *SI Appendix*). These measurements show that the average height of short dsDNA tethered to a surface and able to freely rotate is approximately half of its fully extended length, and they also confirm CSOP's ability to accurately capture a broad range of molecular heights.

As a test of CSOP's height resolution, we measured the thickness of lipid bilayers formed from either 14- or 20-carbon lipids. We compared the average position of one fluorophore labeling both leaflets of a supported lipid bilayer on a glass bead to the average position of a second fluorophore labeling only the outer leaflet (Fig. 1*E* and *Materials and Methods*). The difference in radius of the two different labeling schemes reports the thickness of one leaflet. Using this approach on ∼100 beads composed of either 14- or 20-carbon lipids, we were able to detect a difference in lipid leaflet thickness due to acyl chain length of $\langle h \rangle = 0.36 \pm 0.1$ nm (SEM). This gives a difference in bilayer thickness ($2 \times \langle h \rangle$) that is consistent with previous measurements of

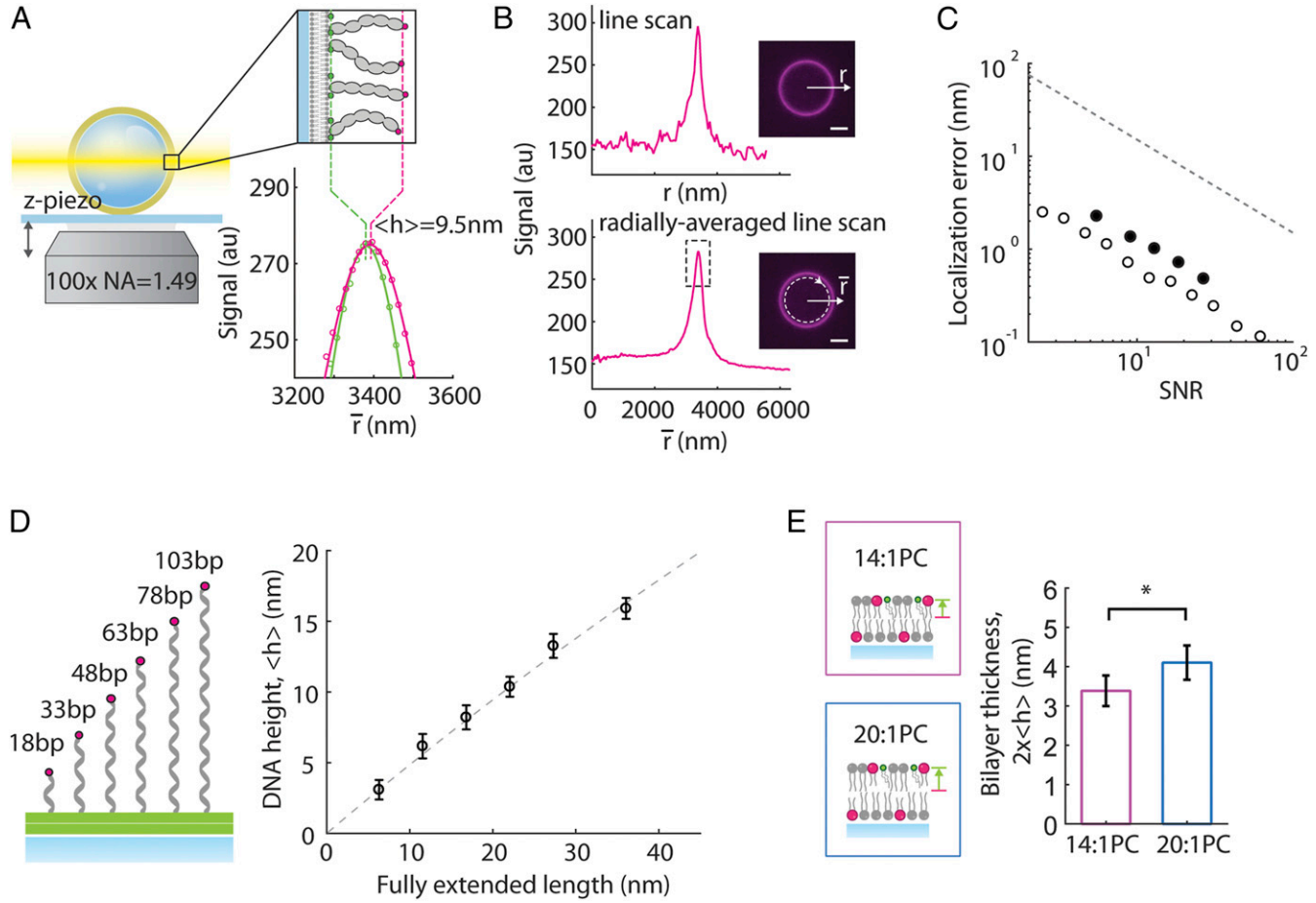

Fig. 1. CSOP measures cell surface molecular heights using two-point localization. (*A*) In an example CSOP measurement, a lipid-coated glass bead (6.8-μm diameter) with multidomain proteins bound to the membrane is imaged using confocal microscopy with a high-NA objective while a z-piezo stage scans the bead through a confocal plane. *Inset* shows a bilayer labeled with green fluorescent dyes and multidomain proteins labeled with red fluorescent dyes at their tip. Protein height, <h>, is measured by localizing the centroids of the green and red fluorescent peaks averaged axisymmetrically. The fluorescence intensities of the protein or lipid channels (red and green circles) and their corresponding Gaussian fits (red and green lines) are shown below. (*B*) A representative fluorescent profile of a protein on a lipid-coated bead (*Insets*) along a single line *r* (*Top*) or by radial averaging $\bar{r}$ of fluorescence signal (*Bottom*), showing the improved SNR with radial averaging. The dashed gray box in *Bottom* line scan is zoomed in *A*. (Scale bar, 2 μm.) (*C*) Comparison of CSOP's resolution (circles) to other single-molecule localization methods (gray dashed line) based on Thompson et al. (29). The open circles were obtained from simulated data, and the closed circles were obtained from experimental data. (*D*) CSOP measurement of surface-tethered dsDNAs of varying length. Dashed line indicates the predicted WLC height when the persistence length is 50 nm, showing good agreement; $n > 40$ for all measurements. The error bar indicates SD. (*E*) Quantification of lipid bilayer thickness with CSOP. *Inset* illustrates the location of a green (TopFluor-Cholesterol) and red (Liss Rhod B) label within a bilayer. The magenta and blue bars show the measurement of a bilayer containing either 14:1PC or 20:1PC lipids, respectively (n = 99 or 103). Error bars indicate the 95% CIs. *P* value is 0.015 based on two-sample Student's *t* test (*$P < 0.05$).

0.066 nm per acyl chain carbon by X-ray diffraction (35) and confirms that subnanometer resolution is possible with CSOP.

Measurement of Multidomain Protein Height and Flexibility with CSOP. To demonstrate the ability of CSOP to measure nanometer-scale differences in the height of multidomain proteins, we constructed a series of FN3 domain repeat proteins (9). The FN3 proteins ranged from a single domain (1L) to 11 domains (11L), with molecular weights ranging from 14 kDa to 154 kDa, respectively. We attached the purified multi-FN3-domain proteins via a His-tag to supported lipid bilayers containing Ni-chelating lipids on a glass bead. We labeled each protein with an N-terminal ybbR-tag, and we labeled the bilayer with an AlexaFluor dye-conjugated His-tag peptide (Fig. 2*A* and *Materials and Methods*). Using CSOP, we measured the heights of each of the multi-FN3-domain proteins and compared them with the estimated fully extended height, which was obtained by multiplying the FN3 domain size based on its crystal structure by the number of domains. As expected for flexible, multidomain proteins, the measured height was consistently shorter than the proteins' maximum fully extended height (Fig. 2*A*).

We next sought to use our measurement of average height to determine the flexibility of the multi-FN3-domain proteins using course-grained MD simulations. We simulated proteins tethered to membranes using a worm-like chain model with a defined persistence length (L_p), which captures the resistance to bending, with $L_p = 0$ representing a freely jointed chain (blue) and $L_p = \infty$ representing a rigid rod (gray) (Fig. 2*B*, *Materials and Methods*, *SI Appendix*, Figs. S4–S6, and Movie S1). Comparing the simulations to the CSOP data, we found that the height measurements for all multi-FN3-domain proteins were consistent with simulations of a semiflexible polymer with $L_p \approx 12.6$ nm (red), indicating that the orientation of the synthetic multi-FN3-domain proteins is highly correlated (rod-like) over approximately three domains.

We then used CSOP to measure the height of a series of native multidomain cell surface proteins whose average height and flexibility were not previously known (Fig. 2*C*). Specifically, we measured mouse signal regulatory protein alpha (SIRPα) (three

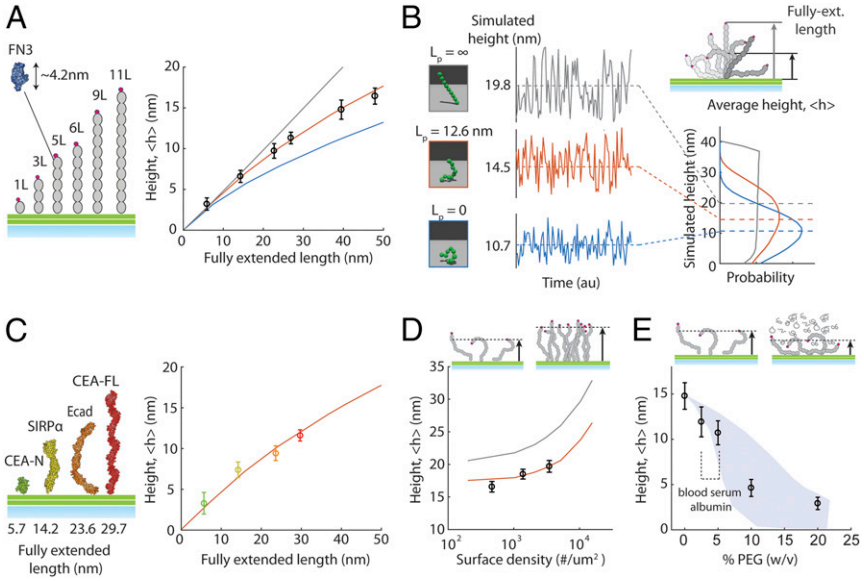

Fig. 2. CSOP measurements of multidomain proteins' height and flexibility. (*A*) CSOP height measurements of a series of multi-FN3-domain proteins. The lines indicate MD simulation of a rigid rod (gray), a semiflexible polymer with the persistent length 12.6 nm (red), and a freely jointed chain (blue). The size of a single FN3 domain is assumed to be 4.2 nm based on its structure (Protein Data Bank [PDB] 3TEU); $n > 25$ for all proteins. (*B*) (*Left*) MD simulations of a 9L FN3 domain protein height with different persistence lengths vs. time. The dashed lines indicate the mean height. The graphics show an instantaneous protein configuration. (*Top Right*) Illustration of a protein on a membrane surface while bending and rotating. (*Bottom Right*) Protein height probability distributions of the 9L FN3 domain based on MD simulations. (*C*) Height measurements of native cell surface proteins human CEACAM5 N-terminal domain (CEA-N), mouse SIRPα (PDB 2wng), mouse E-cadherin (PDB 3q2v), and human CEACAM5 full-length protein (CEA-FL; PDB 1e07). Fully extended lengths are based on crystal structures. The red line indicates an MD simulation of a semiflexible polymer with persistence length 12.6 nm, same as in *A*; $n > 25$ for all measurements. (*D*) Average height measurements of 11L FN3 domain protein at three different surface densities up to the packing density limit (10, 40, and 180 nM in solution); $n = 92$, 50, and 79, respectively. The curves show MD simulation results for a rigid rod (gray) and a semiflexible polymer with the persistence length 12.6 nm (red). (*E*) Average height of 9L FN3 domain protein is measured with varying concentrations of PEG8K in solution. The dashed line indicates physiological concentration of blood serum albumin. The shaded area shows MD simulation results when the radius of gyration of PEG8k was varied from 2.6 nm to 3.5 nm; $n > 15$ for all measurements. The error bars in all figures indicate SD.

Ig domains), mouse E-cadherin (five cadherin domains), and human carcinoembryonic antigen-related cell adhesion molecule 5 (CEACAM5) full-length protein (seven Ig-like domains), as well as the N-terminal domain of CEACAM5 alone (one Ig-like domain). For the extracellular domain of each protein, we added an N-terminal ybbR-tag for fluorescent labeling and a C-terminal His-tag for membrane binding. Similar to our measurement of multi-FN3-domain proteins, all four proteins behaved as worm-like chains with average heights shorter than their fully extended height. Interestingly, all measured proteins were well described by a semiflexible polymer with $L_p \approx 12.6$ nm, suggesting similar flexibility of these proteins and the multi-FN3-domain proteins. These data show that CSOP measurements combined with simulations can provide critical information on the height and flexibility of cell surface proteins that cannot be obtained from crystal structures.

Effect of Surface and Solution Crowding on Multidomain Protein Height. We next used CSOP to measure the effect of surface density on protein height. Molecular crowding of proteins on a membrane surface can create significant lateral pressure (36) that can alter the height of multidomain proteins by constraining their fluctuations, as in the case of densely crowded MUC1 glycoproteins on the surface of epithelial cells (10). To quantify the effect of protein crowding on height with CSOP, we measured our longest multi-FN3-domain protein (11L) at three different surface densities. We found that the average height of the protein increased significantly, by 1.9 nm (11%) and 3.1 nm (19%), as surface densities increased by a factor of 3× and 7.5×, respectively, from an initial density of ~460/μm^2 (Fig. 2*D*). This change is consistent with our MD simulations for those densities, and we predict that protein height can increase by up to 50% at surface densities equivalent to that of native cell membranes (>10,000/μm^2) (3) (*Materials and Methods*).

Cell surface proteins experience not only lateral crowding from neighboring membrane-bound proteins but also macromolecular solution crowding from the surrounding medium. We used CSOP to detect the effect of solution crowding on height, by measuring a long multi-FN3-domain protein (9L) under varying amounts of 8-kDa polyethylene glycol (PEG) in solution. Interestingly, we found that protein height decreased by 20 to 30% for solution crowding concentrations of 3.5 to 5% wt/vol, which are physiological levels of solution crowding concentration (37), with more dramatic height decreases for solution crowding concentrations exceeding 5% wt/vol (Fig. 2*E*). Again, our measurements agreed well with results from MD simulations of solution crowding, which also predict that the absolute height decrease by bulk osmotic compression is larger for taller proteins than for shorter ones (*Materials and Methods* and Movie S2). Our data suggest that physiological concentrations of macromolecules in solution will affect not only the height of the thick glycocalyx (100 nm to 500 nm) of epithelial (38) or endothelial (39) cells but also the height of cell surface proteins on nearly all cells.

Measurement of Protein Height Using Antibodies. While CSOP requires a fluorescent marker at the tip of a cell surface molecule to measure its height, that marker need not be an engineered fluorescent tag. Indeed, for CSOP to be broadly useful for measuring cell surface proteins on primary cells, such as patient samples, an approach that does not require modification of native proteins is needed. Here we demonstrate the use of fluorescent antibodies targeting the terminal domain of surface proteins to enable protein height measurements on native cell membranes.

To validate antibody labeling, we first measured the heights of CEACAM5, SIRPα, and multi-FN3-domain proteins with antibodies targeting their terminal domains and compared those to measurements of the same proteins with engineered fluorescent tags on their terminal domains (Fig. 3*A*). We observed that antibodies add an offset of 1.5 ± 1.4 nm (SD) to CEACAM5 and a larger offset for shorter proteins. We expected the antibody to add height because cross-linking by the antibody constrains the target protein to be taller (*SI Appendix*, Fig. S7) and the antibody is, itself, a relatively large molecule (~7 nm for the Fab). To quantify the expected height increase, we used MD simulations of antibody–protein complex motion and found that steric effects result in an increase in apparent height of ~1.6 nm (*Materials and Methods*, *SI Appendix*, Fig. S8, and Movie S3). This offset increases as protein size decreases, which is consistent with our experimental measurements with CSOP (Fig. 3*A*). The same trend in offset was observed regardless of a target protein's flexibility or surface density in the simulations, suggesting that protein height can be accurately measured with a fluorescently labeled antibody by subtracting the height-dependent offset added by the antibody. Other antibody types composed of only one Ig domain (e.g., nanobody) or two Ig domains (e.g., bivalent nanobody, single-chain variable fragment) can also be used to label and measure the height of a cell surface protein with CSOP. Using MD simulation, we found that the offset added by these antibody types is significantly smaller than that added by the full-IgG antibody (*SI Appendix*, Fig. S8).

Measurement of Antibody Epitope Location on a Multidomain Protein. Identifying antibody epitopes usually requires cocrystallography, mutagenesis and binding measurements, or cross-linking coupled mass spectrometry (40), all of which are time-consuming and costly methods. We wondered whether CSOP could be used to determine the approximate location of antibody epitopes on multidomain proteins by measuring the antibody height and comparing it to protein height.

As a demonstration of epitope mapping with CSOP, we examined antibodies targeting CD45—a transmembrane tyrosine phosphatase whose exclusion from membrane interfaces plays a critical role in immune cell activation (41, 42) (Fig. 3*B*). The CD45 extracellular domain comprises an N-terminal mucin-like region followed by a cysteine-rich domain (d1) and three fibronectin type 3 (FN3) (d2 to d4). The longest human CD45 isoform, $CD45R_{ABC}$, has a mucin-like region of 202 residues and is predicted to be ~40 nm when fully extended, with domains d1 to d4 accounting for 15 nm of its height (42, 43).

We used four commercially available anti-CD45 antibodies that have different isoform specificities and are therefore thought to bind at different locations to CD45, although the specific epitopes and domain locations are unknown. We selected the pan-CD45 antibodies I3 and 30F11, the anti-$CD45R_B$ antibody C363, and the anti-$CD45R_{ABC}$ antibody B220. Using CSOP, we measured the height of the antibodies on $CD45R_{ABC}$ bound to lipid-coated beads, and we were able to clearly separate the binding locations: I3 bound to the d4 domain (6.1 ± 1.4 nm [SD]), 30F11 bound to the d2 to d3 domain (7.6 ± 1.7 nm [SD]), C363 bound to the proximal part of the mucin-like domain (15.7 ± 1.6 nm [SD]), and B220 bound to the distal part of the mucin-like domain (19.8 ± 1.4 nm [SD]) (Fig. 3*B*). Based on the measurement of the B220 antibody, the $CD45R_{ABC}$ extends an average of 18.2 nm from the membrane surface, less than half the fully extended height estimated from its structure (42, 43). These results suggest that antibody binding sites separated by ~1 nm within the same protein are resolvable using CSOP.

Measurement of Glycan Height on a Multidomain Protein. While we have focused on protein height measurements, the majority of cell surface proteins are glycosylated (44), the extent to which will alter their cell surface height. Importantly, glycosylation is not typically accounted for in crystal structures and is difficult to predict for a given protein, making direct measurement of glycans the most reliable way to determine their height. We tested CSOP's ability to localize cell surface glycans using lectins that bind to specific glycans.

Using the purified extracellular domain of $CD45R_{ABC}$, we measured the height of fluorescent plant lectins Soybean Agglutinin (SBA), which binds GalNAc and galactose, and Sambucus Nigra Lectin (SNA), which targets α-2,6 sialic acids, on $CD45R_{ABC}$ (Fig. 3*C*). We found that the average height of SNA was 13.8 ± 1.6 nm (SD), while the average height of SBA was 8.3 ± 1.7 nm (SD). SNA was localized close to the height of the anti-$tCD45R_B$ antibody epitope, suggesting that $CD45R_{ABC}$ is predominantly sialylated in the mucin-like domain. Our measurements demonstrate that CSOP can capture differences in the average position of specific glycans on the same molecule.

Measurement of Glycoprotein Height on Native Cell Membranes. We next applied CSOP to make high-resolution molecular height measurements on native cell membranes. While the use of antibodies to target endogenous cell surface proteins is compatible with CSOP, as demonstrated above, the arrangement of cell membranes in a spherical geometry is necessary to make use of radial averaging. Conveniently, several techniques have already been devised for preparing cells and cell membranes that are compatible with CSOP measurements, including giant plasma membrane vesicles (GPMVs) (45) and swollen cells (46). Despite some drawbacks arising from the preparation of GPMVs (47), both GPMVs and swollen cells allow for measurement of native cell surface proteins including their posttranslational modification.

To test whether CSOP can accurately measure molecular heights on GPMV (45), we compared the height of a protein we had previously measured on the supported bilayer of a lipid-coated glass bead, CEACAM5, to CSOP measurement of GPMVs from cells overexpressing CEACAM5 (Fig. 4*A* and *Materials and Methods*). GPMVs maintain the native lipid and protein diversity, allowing biochemical and biophysical studies of cell membrane and proteins separate from the cytoskeleton. We labeled CEACAM5 using a bivalent V_{HH} nanobody that recognizes a small peptide tag at its N terminus (48). Based on CSOP height measurements, we found that CEACAM5's height in GPMVs was consistent with its height measured in lipid-coated beads (Fig. 4*B*). We repeated GPMV measurements for the CEACAM5 N-terminal domain alone, as well as SIRPα and E-cadherin, all using the V_{HH} nanobody, and we found that average height measurements from the GPMVs were remarkably consistent with those from lipid-coated beads, except for SIRPα, which was 40% higher when measured in a GPMV (Fig. 4*C*). We wondered whether the way in which SIRPα was attached to the membrane—with a transmembrane domain in native cell membranes compared to a His-tag on the extracellular domain in vitro—could affect the measured height. To test the effect of membrane attachment, we swapped the wild-type transmembrane domain of SIRPα for a glycosylphosphatidylinositol (GPI) anchor. Interestingly, the height of SIRPα GPI in GPMV exhibited only 27% increase from its height measured in lipid-coated beads, compared to 40% increase with the wild-type transmembrane domain (Fig. 4*C*). This suggests that the transmembrane anchor can significantly change protein height, in addition to other factors, showcasing the sensitivity of CSOP measurements for structural details of cell surface molecules.

Since some cell types are not amenable to GPMV formation, we adapted an existing protocol for osmotically swelling cells into spheres for use with CSOP (46) (Fig. 4*A*). To swell cells, we first disrupt the actin and microtubule cytoskeleton by using small-molecule drugs, Latrunculin A and Y-27632 (*Materials and*

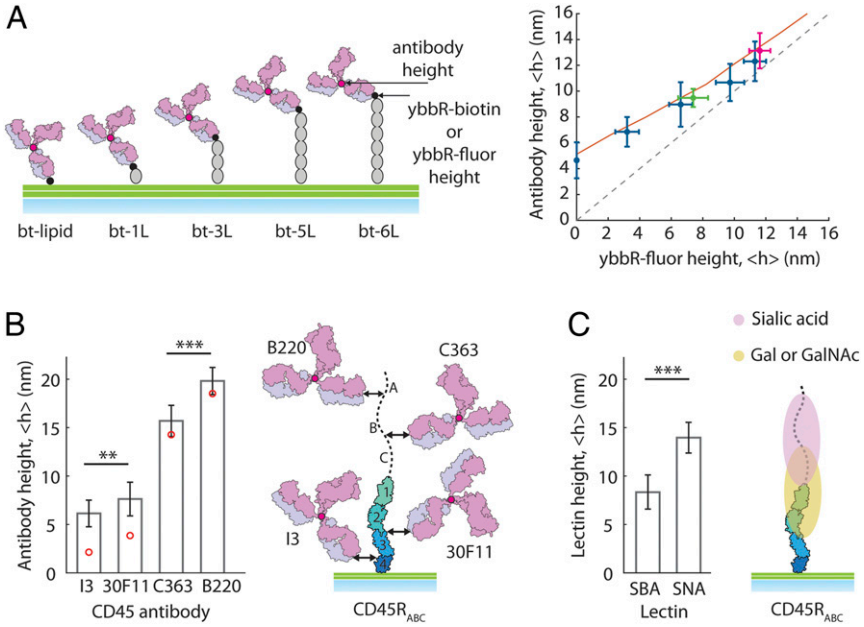

Fig. 3. CSOP measurements of protein and glycan heights using fluorescent antibodies and lectins. (*A*) Biotinylated (ybbR-biotin) multi-FN3-domain proteins (bt-1L to bt-6L) were labeled with fluorescently labeled anti-biotin antibodies, as was a biotinylated lipid (bt-lipid). Black dots indicate biotin or engineered fluorescent tag, and red dots indicate the antibody's center of mass. Each antibody is labeled at multiple positions without site specificity, making the antibody center of mass a good approximation of the antibody location. Height measurements based on localizing the fluorescent antibody of the multi-FN3-domain proteins (*y* axis, blue) are plotted against the protein height based on an engineered fluorescent tag (ybbR-fluor, *x* axis), showing a size-dependent offset. Measurement of SIRPα (green) and CEACAM5 (magenta) are consistent with the multi-FN3-domain protein measurements. The red line indicates result from MD simulations, and the dashed line shows a case whereby the antibody location is identical to the protein height; $n > 25$ for all measurements. (*B*) Height measurement of antibodies bound to CD45R$_{ABC}$. Red circles indicate epitope height after subtracting the offset added by the antibody; $n > 20$ for all measurements. *P* values based on two-sample Student's *t* test are 0.002 and 3.5×10^{-11} (**$P < 0.01$, ***$P < 0.001$). The measured heights of anti-CD45 antibodies are mapped onto a model of CD45R$_{ABC}$, showing the predicted locations of the antibody epitopes (black arrows). (*C*) Height measurement of lectins bound to CD45R$_{ABC}$; $n > 20$ for all measurements. All error bars indicate the SD. *P* value based on two-sample Student's *t* test is 4.2×10^{-14}. The measured heights of glycans are mapped onto a model of CD45R$_{ABC}$, showing a difference in the height of sialic acid and Gal/GalNAc residues.

Methods). Next, we hydrostatically swell cells by reducing the extracellular buffer osmolarity. More than 50% of HEK cells overexpressing CEACAM5 turned completely spherical at ∼80 mOsm and remained swollen for at least 1 h without any volume decrease (49). After cell swelling, we labeled the membrane using a CellMask dye and labeled CEACAM5 using the V_{HH} nanobody, as above. Fluorescently labeled CEACAMs were uniformly distributed on the membrane, making it indistinguishable from a GPMV. We then measured protein height and found that CEACAM5's height on a swollen cell is ∼10% higher than its height measured on a lipid-coated bead (Fig. 4*B*). This is consistent with our previous observation that multi-FN3-domain proteins are more extended at high surface densities, like those expected on a native cell membrane (Fig. 2*D*).

Measurement of Proteome and Glycome Heights on Native Cell Membranes. Height measurements based on antibodies and engineered tags can provide information on specific cell surface molecules, but it is often useful to know how tall the surrounding molecules are in comparison. This is particularly relevant when considering, for example, whether an antibody-bound antigen on a tumor cell is accessible to an immune receptor.

To explore this, we measured average cell surface proteome and glycome heights on an HER2-positive breast cancer cell, SKBR3, and on a macrophage progenitor cell, Hoxb8 (50). To measure average proteome height, we labeled the N terminus of cell surface proteins using an amine-reactive biotin (*N*-hydroxysuccinimide [NHS]-Biotin) at low pH (pH 6.5) (51). We then swelled the cells, as described above, and measured the height of the cell surface biotin label using an anti-biotin antibody. The average cell surface proteome height of SKBR3 cells was measured to be 13.5 ± 2.2 nm (SD), and that of the Hoxb8 cell was found to be 15 ± 2.9 nm (SD). To determine the average cell surface glycome height, we used CSOP to measure the heights of GlcNAc and sialic acid with the lectins Wheat Germ Agglutinin (WGA) and Maackia Amurensis Lectin II (MAL-II), respectively. The average heights of α-2,3 sialic acid as measured by MAL-II were 16.4 ± 3.7 nm (SD) (SKBR) and 16.7 ± 2.6 nm (SD) (Hoxb8) (Fig. 5). We also found that GlcNAc heights as measured by WGA were 7.8 ± 1.9 nm (SD) (SKBR) and 5.9 ± 1.8 nm (SD) (Hoxb8).

In order for an immune cell to recognize and act on a tumor cell, it must be able to bind to a target molecule on the tumor cell surface, such as an antibody-bound antigen. To determine whether the measured proteome and glycome heights present a physical barrier to that binding, we measured the height of the therapeutic antibody target HER2 using the anti-HER2 antibody Trastuzumab, the antibody-binding receptor FcγR, and the phosphatase CD45R$_{ABC}$, which must be excluded for FcγR activation (Fig. 5). We found that the height of CD45R$_{ABC}$ on Hoxb8 cells was 24.7 ± 1.3 nm (SD), significantly exceeding the average total protein and glycan height, which would enable it to be excluded when the cells come into close contact. However, the measured heights of the therapeutic antibody Trastuzumab (7.9 ± 1.4 nm [SD]) and FcγR (6.2 ± 1.7 nm [SD]) show that it is well below the average proteome heights on the native cell surface. This indicates that accessibility of HER2 and FcγR may be sterically limited by surrounding proteins. While these data are for cultured cells, our results suggest that variations in cell surface height profiles of tumor cells and immune cells in patients could significantly affect the accessibility of tumor antigens and the efficacy of antibody-mediated immunotherapies.

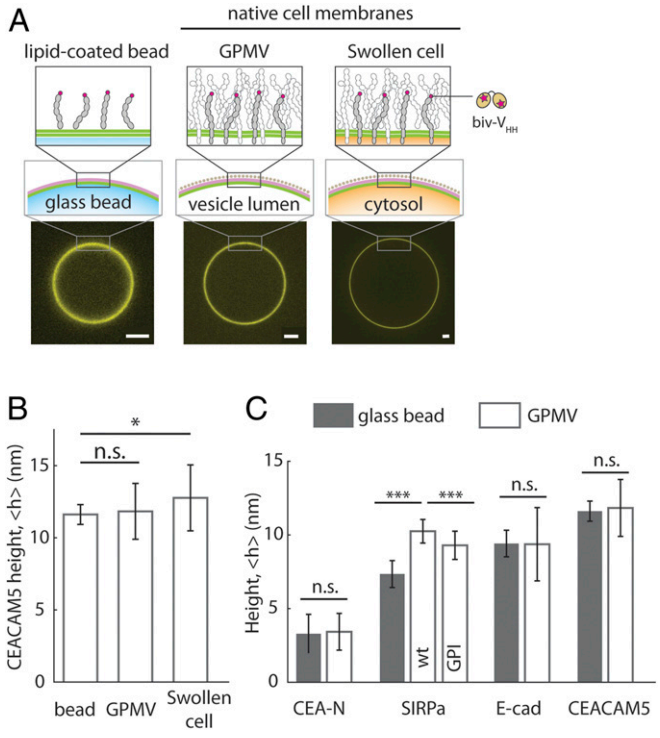

Fig. 4. CSOP measurements of cell surface protein heights in native membranes. (*A*) Illustration of protein and membrane preparations that can be measured with CSOP. For the measurement in a lipid-coated bead, a protein's N-terminal ybbR-tag is enzymatically labeled with an Alexa dye. In a GPMV and a swollen cell, a bivalent V_{HH} nanobody (biv-V_{HH}) is bound to a protein's N-terminal SPOT-tag. Biv-V_{HH} introduces the offset of less than 1 nm to CEACAM5 (*SI Appendix*, Fig. S8). Images show fluorescent CEACAM5 in the different preparations. (Scale bar, 2 μm.) (*B*) CSOP measurement of CEACAM5 in three different preparations; $n = 30$, 40, and 26, respectively. The bead diameter is 6.8 μm. *P* values based on two-sample Student's *t* test are 0.56 and 0.011, respectively (n.s. = $P > 0.05$, *$P < 0.05$). (*C*) Measurement of cell surface protein heights on lipid-coated beads (the closed columns) versus GPMVs (the open columns). *P* values based on two-sample Student's *t* test are 0.63, 4.7×10^{-19}, 7.0×10^{-4}, 0.92, and 0.56, respectively (n.s. = $P > 0.05$, ***$P < 0.001$); $n > 15$ for all measurements.

Discussion

The cell surface landscape plays an important role in diverse cellular processes. Since small changes in the height of molecules can significantly alter receptor binding and glycoprotein exclusion from cell–cell interfaces, quantifying the height of molecules comprising the cell surface proteome and glycome with nanometer-scale resolution is important for a mechanistic understanding of cell–cell interactions.

We have developed a superresolution localization-based method called CSOP that can rapidly and simply measure protein and glycan heights with nanometer resolution on native cell membranes. We applied this technique to measure membrane thickness, quantify the height and flexibility of purified proteins as well as native proteins, and test the effect of surface and solution crowding on protein heights. Our all-optical approach can be multiplexed to simultaneously quantify the heights of multiple molecules in a matter of minutes with conventional spinning disk confocal microscopy, overcoming challenges with current methods that limit resolution, require extensive preparation time, or are not compatible with unfixed, native cell membranes.

CSOP takes the localization concept that enables 3D superresolution imaging and trades lateral resolution for improved vertical resolution. Rather than the maximum practical resolution of ∼10 nm for PALM, STORM, and stimulated emission depletion microscopy, CSOP is able to quantify average cell surface protein height with ∼1-nm resolution by averaging multiple molecules reporting the same heights. In addition to its resolution, CSOP sample preparation is simple, and the measurement is rapid. When measuring a native protein with commercially available antibodies, the cell preparation, surface labeling, calibration, measurement, and data analysis can be completed within 3 h to 5 h.

Although CSOP uses the straightforward concept of fluorophore localization, achieving nanometer-scale height resolution on native membranes required several developments to enable robust and reliable measurements. First, we established a calibration protocol and membrane labeling strategy to localize membrane and proteins without errors associated with chromatic aberration or fluorescence polarization, allowing CSOP to maintain high resolution even with modest acoustic vibration (*SI Appendix*, Fig. S9). Second, we validated the accuracy of average height measurement using dsDNAs and MD simulations. Third, we quantified the offset introduced by antibody labeling, enabling height measurements and antibody epitope mapping of unmodified cell surface proteins, such as those on primary cells. Lastly, we confirmed that existing methods for preparing native cell membranes, including GPMVs and cell swelling, can be adapted to CSOP for the measurement of cell surface proteins on native cell membranes.

As shown above, CSOP has the potential to be a broadly useful tool for investigating diverse biological processes including protein isoform changes during cell differentiation (52), modifications in glycan height during cancer progression (26), and kinetics of protein conformation changes (53). Ongoing developments in protein labeling strategies using antibodies and site-specific chemical labels have the potential to improve the ability of CSOP to quantify the height and flexibility of cell surface molecules and their functional consequences.

Materials and Methods

Expression, Purification, and Fluorescent Labeling of Proteins. Multi-FN3-domain proteins containing N-terminal ybbR-tags and C-terminal His10-KCK-His6 were expressed and purified as described previously (9). Briefly, FN3 proteins were expressed in Rosetta DE3 competent cells (EMD Millipore), lysed by sonication, and affinity-purified over a His-Trap HP column (GE Healthcare). The proteins were gel-filtered, and their size was validated via a Superdex 200 column on an AKTA Pure system (GE Healthcare). We labeled 50 μM protein using 10 μM SFP synthase [purified according to published protocols (54)], 40 μM AlexaFluor dye-conjugated CoA, and 10 mM $MgCl_2$. The conjugates were then gel-filtered via a Superdex 75 10/300 GL column. Labeling efficiencies of 60 to 90% were obtained.

The extracellular human CEACAM5 N-terminal domain (Lys35 to Leu144) and full-length proteins (Lys35 to Ser677, Uniprot P06731) or mouse SIRPα (Lys32 to Asn373, Uniprot P97797) were cloned into a pCAGGs vector, with the native signal sequence, an N-terminal ybbR-tag for labeling, and C-terminal His10 for affinity purification. The extracellular mouse E-cadherin (Asp1 to Asp533 of the mature, furin-processed protein, Uniprot P09803) was cloned into a pCAGGs vector, with a human CD33 signal sequence replacing the native signal peptide, a TEV protease cleavage sequence (ENLYFQG) immediately followed by an N-terminal Sortase-A tag for labeling (Gly5 including the TEV sequence), and C-terminal His10 for affinity purification. For all proteins, a T175 flask of HEK293T cells was transfected with TransIT-293 (Mirusbio) per vendor's protocol and incubated in Dulbecco's modified Eagle's medium containing 10% fetal bovine serum. Proteins were-affinity purified from the supernatant 48 h posttransfection over a HisTrap Excel column (GE Healthcare). We used sodium phosphate buffer (20 mM Na phosphate, 0.5 M NaCl, pH 7.4) for CEACAM and SIRPα purification and Hepes buffer (50 mM Hepes, 150 mM NaCl, pH 7.4) containing 3 mM $CaCl_2$ for E-cadherin purification. We labeled CEACAM and SIRPα using SFP synthase as above and gel-filtered the conjugates via a Superdex 75 10/300 GL column. We labeled E-cadherin with Sortase-A using the custom peptide probe (the peptide CLPETGG [Genscript custom peptide synthesis, >95% purity] conjugated with AlexaFluor dyes). The N-terminal Sortase-A tag was exposed by TEV protease immediately before labeling (protein to TEV ratio 1 to 20) to achieve high labeling efficiency, and the labeling was

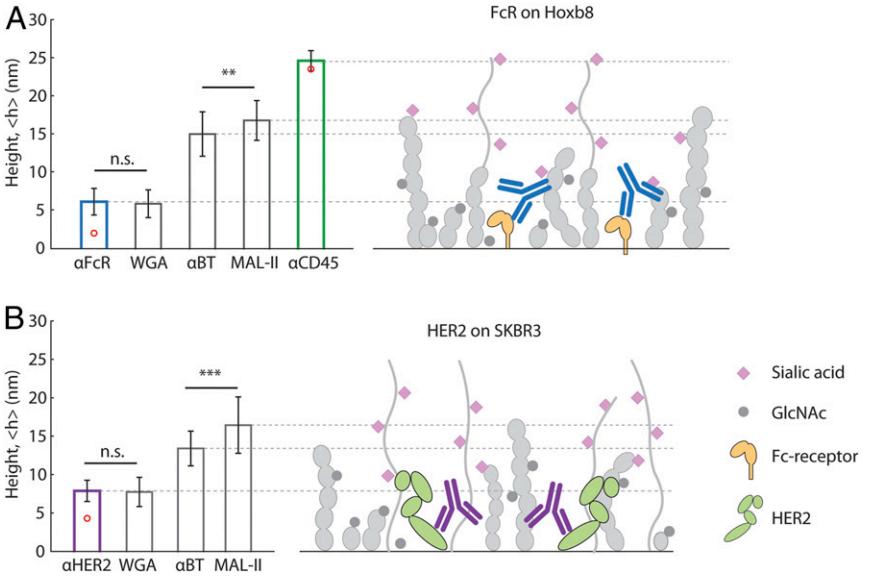

Fig. 5. CSOP measurements of average cell surface proteome and glycome heights on tumor and immune cells. (*A*) The heights of Fc receptor, CD45, average proteome, and average glycome were measured on Hoxb8 cells by binding antibodies or lectins. The results indicate that Fc receptors are much shorter than the average proteome and some glycan structures. Anti-biotin, Anti-CD45, and lectins are not drawn; $n > 30$ for all measurements. Error bars indicate SD. *P* values based on two-sample Student's *t* test are 0.66 and 5.0×10^{-5} (n.s. = $P > 0.05$, $^{**}P < 0.01$). (*B*) The height of HER2, average proteome, and average glycome were measured on SKBR3 tumor cells by binding antibodies or lectins. The results indicate that Her2 are buried compared to the average proteome and some glycan structure. Anti-biotin and lectins are not drawn; $n > 30$ for all measurements. All error bars indicate the SD. *P* values based on two-sample Student's *t* test are 0.54 and 0.0085 (n.s. = $P > 0.05$, $^{***}P < 0.001$).

conducted according to the published protocol (55). The conjugates were then gel-filtered via a Superdex 75 10/300 GL column. Labeling efficiency was 65% or higher for all proteins.

Microscope for CSOP Height Measurements. CSOP imaging was carried out on an inverted Nikon Eclipse Ti microscope (Nikon Instruments) equipped with a Yokogawa CSU-X spinning disk using an oil-immersion objective (Apo TIRF 100×, NA 1.49, oil). Three solid-state lasers were used for excitation: 488, 561, and 640 nm (ILE-400 multimode fiber with BCU, Andor Technologies). The laser power at the sample plane was less than 1.5 mW for all three channels. Fluorescent light was spectrally filtered with emission filters (535/40m, 610/75, and 665LP, Chroma Technology) and imaged on an sCMOS camera (Zyla 4.2, Andor Technologies). Z stack was acquired using a piezo z stage (npoint).

Calibration of CSOP Height Measurements to Account for Chromatic Aberrations. Prior to making CSOP measurements, a calibration procedure was run to account for the chromatic aberrations specific to the sample and to the microscope configuration (*SI Appendix*, Fig. S2). The calibration begins with taking a Z stack of a sample, for example, lipid-coated glass bead, with the two fluorophores to be used for the height measurement both labeling the same lipid bilayer, which should give a height measurement of zero. Based on the images, we calculate the radius of fluorophores in each z slice using a custom MATLAB script (see *Protocol for CSOP Data Analysis*) and determine the maximum radius in each color at the bead equator. The offset between the measured fluorescent radii (h_{offset}) results solely from the chromatic aberration, providing a parameter that can be used to compensate subsequent measurements. When the measured height, $h_{measured}$, of a cell surface molecule is obtained by quantifying the difference in radii of the fluorescently labeled bilayer and tip of the surface molecule, the aberration corrected average height, <h>, can be calculated as $\langle h \rangle = \langle h_{measured} \rangle - \langle h_{offset} \rangle$.

The calibration offset measured for a specific sample remains almost constant (~1-nm drift over a week) for a system with the same optical configuration. However, the offset varies significantly depending on the type of sample due to the difference in the refractive index (RI) of the buffer, RI mismatch between the spherical sample and the buffer, the size of the sphere, and the polarization of the fluorophore labeling membranes (see below). For this reason, the sample-specific calibration is performed when a new type of sample is measured.

Method for Avoiding Polarization Effects. Separate from the chromatic aberration, polarization effects of fluorophores labeling lipid membranes can also induce a nonzero $\langle h_{offset} \rangle$ for beads of diameter 8 μm or less. The majority of lipid–fluorophore conjugates are highly oriented by the bilayer, leading to errors in the correction of cell surface molecular height measurements (33). To avoid this, we used an AlexaFluor dye conjugated to a His-tag that binds to the surface of Ni-containing bilayers in place of lipid–fluorophore conjugates to localize the bilayer surface (*SI Appendix*, Fig. S3).

Protocol for CSOP Height Measurements. CSOP sample preparations are described in the sections below. The samples were loaded on a custom imaging chamber, which was made by adhering a polydimethylsiloxane well to a 1.5 coverslip (Thermo Fisher Scientific). The coverslip was passivated by forming a supported lipid bilayer or by adsorbing bovine serum albumin while presenting binding molecules such as Cell-Tak for immobilizing CSOP samples. Prior to CSOP imaging, the laser power and exposure time were adjusted in both channels. In general, a <1-mW laser power at the sample plane and an exposure time shorter than 200 ms provided an SNR of ~10 or higher in both fluorescence channels. We kept the SNR of two fluorescence channels identical to avoid any potential bias to CSOP measurement. We manually determined the equator of samples and acquired ~20 slices of images with a 50- to 100-nm step size using the z-piezo stage. We collected images in two fluorescence channels before moving the z position, but collecting the Z stack of each fluorescence channel separately did not affect the results. Each Z-stack image contained up to 10 spherical samples per field of view.

Protocol for CSOP Data Analysis. We used a custom MATLAB (Mathworks) script to estimate the radius of samples from CSOP images (56). The algorithm radially averages fluorescent signals from the center of a circle to construct the 1D signal distribution in the radial direction. To determine the center of a circle accurately, we performed the radial averaging in 900 different center locations and quantified the height of radial profile at its peak. We then created the two-dimensional (2D) map of peak heights versus centers and fit the 2D Gaussian surface to estimate the true center, where the peak height becomes maximized. To determine the peak location of the radial profile from the center, which corresponds to the radius of CSOP sample, we fit the Gaussian curve to the top 10% region of the peak.

Measurement of Lipid Bilayer Thickness. To create a lipid-coated bead, first, small unilamellar vesicles (SUV) were formed according to published protocols (9). To calibrate the measurement baseline, a lipid film composed of 20:1PC, 2.5 mol% Ni- nitrilotriacetic acid (NTA), 0.15 mol% 1,2-dioleoyl-*sn*-glycero-3-phosphoethanolamine (DOPE)–Lissamine Rhodamine B (Liss Rhod B), and 1 mol% TopFluor-Cholesterol was rehydrated with Milli-Q (MQ) water to 0.2 mg/mL, sonicated at low power (20% of max), added to Mops buffer (final concentration, 50 mM Mops pH 7.4, 100 mM NaCl), and filtered through a 200-nm PTFE filter (Millipore). Next, 10 μL of 6.8-μm glass bead slurry (10% solid) were cleaned using a 3:2 mixture of H_2SO_4:H_2O_2 (30 min in bath sonicator) and cleaned three times in MQ water. Finally, 5 μL of clean bead slurry were added to 50 μL of SUV solution and mixed gently by pipetting. The bead/SUV mixture was incubated for 15 min at room temperature before the mixture was washed with Hepes buffer (50 mM Hepes pH 7.4, 100 mM NaCl) three times by gentle siphoning. CSOP measurement was performed to determine the offset between bilayer midplanes measured by TopFluor versus Liss Rhod B. To measure bilayer thickness, lipid-coated beads containing only Liss Rhod B were formed. The lipid-coated beads were subsequently incubated with TopFluor-Cholesterol in solution, which spontaneously incorporates into the bilayer's outer leaflet. Twenty-five micromolar TopFluor-Cholesterol was first mixed with 50 μM Methyl-β-cyclodextrin to make the cholesterol compound soluble in buffer. By comparing the locations of TopFluor-Cholesterol (midplane of bilayer) versus Liss Rhod B (surface of bilayer), we determined bilayer leaflet thickness. We performed the measurement for the lipid composed of 14:1PC as well as 20:1PC.

Measurement of DNA Length. The 6.8-μm lipid-coated beads were formed using lipids composed of 1,2-dioleoyl-*sn*-glycero-3-phosphocholine (DOPC), 3.5 mol% Ni-NTA, and 14:0-(*N*-(7-nitrobenz-2-oxa-1,3-diazol-4-yl)-1,2-dihexadecanoyl-*sn*-glycero-3-phosphoethanolamine (NBD PE). The beads were incubated with the size standard DNAs (*SI Appendix*, Table S2) containing an Atto555 dye on one end and cholesterol on the other in buffer containing 150 mM Hepes and 300 mM NaCl for 10 min before imaging. We added varying amounts of DNA to obtain the same surface density between DNA standards. For example, 1 nM of 15 bp or 50 nM of 105 bp provided comparable surface density of ∼1,000/μm^2. The surface density of DNA was estimated based on the fluorescence intensity according to a custom calibration (*SI Appendix, SI Materials and Methods*). The location of membrane surfaces was measured by binding AlexaFluor 555-conjugated deca-histidine peptides to the Ni-NTA lipids. The probe was created by conjugating the thiol-reactive AlexaFluor maleimide dyes and peptides with sequence His10-KCK (Genscript custom peptide synthesis, >95% purity).

Measurement of Multidomain Protein Height and Crowding Effects. The 6.8-μm lipid-coated beads were formed using lipids composed of DOPC, 3.5 mol% Ni-NTA, and 14:0-NBD PE. The beads were incubated with 10 nM of FN3 single-domain or multidomain protein containing an AlexaFluor555 dye at its N terminus and an H10-kck-H6 tag at its C terminus in Hepes buffer (50 mM Hepes and 100 mM NaCl, pH 7.4) for 20 min before imaging. The surface density of proteins was ∼500/μm^2 for all sizes measured. The surface density of proteins was estimated based on the fluorescence intensity according to a custom calibration (*SI Appendix, SI Materials and Methods*). The location of membrane surfaces was measured by binding AlexaFluor 555-conjugated deca-histidine peptides to Ni-NTA lipids. To test the effect of protein surface crowding on height, we bound 11XFN3 proteins at 10, 40, and 180 nM, which provided surface density of ∼460/μm^2, 1,380/μm^2, and ∼3,470/μm^2. To test the effect of PEG in solution on protein height, we made lipid-coated beads using lipids composed of DOPC, 5 mol% DOPS, 5 mol% 18:1 1,2-dioleoyl-*sn*-glycero-3-phosphoethanolamine-*N*-[4-(*p*-maleimidophenyl)butyramide] (MPB-PE), and 14:0-NBD PE. We then covalently bound 9XFN3 proteins to the bilayer using their C-terminal cysteines by incubation for 1 h at room temperature. This was important, because proteins bound via histidine–nickel interactions became unbound quickly after PEG addition. Following protein binding, PEG8k was added to solution to a final concentration of 2.5%, 5%, 10%, or 20% wt/vol before imaging.

Measurement of Protein Heights Using Antibodies and Lectins. All of the antibodies and lectins are fluorescently labeled at their Lysine residues using the AlexaFluor-NHS. Each antibody is conjugated with three to five dyes, and each lectin is conjugated with approximately four dyes (approximately one dye per each monomer). SPOT V_{HH} is a bivalent nanobody randomly labeled with Atto488 with a labeling ratio of one to two dyes per molecule. The high labeling ratio combined with the lack of the labeling site specificity allows us to assume the center of mass of the molecule as its location.

Measurement of Multidomain Protein Height on GPMVs. RBL cells overexpressing a recombinant protein containing an N-terminal SPOT-tag were created by lentiviral transduction (*SI Appendix*). GPMV were formed by adding 25 mM paraformaldehyde and 2 mM dithiothreitol to cells (45). GPMVs were collected within 1 h and subsequently incubated with 1 μg/mL of SPOT V_{HH} conjugated with Atto488 and cholera toxin subunit B-AlexaFluor555 for 20 min at room temperature before imaging. SPOT V_{HH} is a bivalent nanobody that tightly binds to the peptide tag (PDRVRAVSHWSS) introduced at the N terminus of proteins (dissociation constant = 6 nM). GPMVs remained taut throughout imaging.

Measurement of Multidomain Protein Height on Swollen Cells. HEK293T, HOXb8, SKBR3, and MDA-MB-453 cells were used in swelling experiments. Cells were lifted by shear and transferred to an imaging chamber coated with Cell-Tak cell adhesive according to the manufacturer protocol. Cells were loaded at a density where single cells were well separated and then allowed to gently adhere to the glass for 10 min at room temperature. Cells were subsequently washed once with PBS, and cytoskeletal drugs were added (Latrunculin A and Y27632 at 1 μM and 10 μM) for 30 min at room temperature or 37 °C. Cells were washed three times with PBS, and labeling reagents, such as a labeled antibodies, lectins, or CellMask, as well as cytoskeletal drugs, were then added for 20 min at 4 °C. Hepes-buffered MQ (pH 7.5) containing cytoskeletal drugs was subsequently added to swell cells. MQ was added in several steps while cells were monitored. Typically, cells were fully swollen in between 1/4 and 1/10 PBS and remained taut for at least 1 h.

Simulation of CSOP Height Measurement Resolution. We numerically simulated CSOP images to test for CSOP resolution and its sensitivity to acoustic vibration, using a custom Matlab script (56). To do this, we generated an image of a circle reflecting a CSOP sample image at the equatorial plane using the 2D Gaussian point spread function with an SD of 130 nm, a camera pixel size of 55 nm, and Poisson shot noise. We first generated a true image of a circle and convoluted the circle with the point spread function. We then added Poisson noise in each pixel by using the original signal as the mean. We created a pair of circle images simulating the membrane and the protein and determined the protein height by estimating the radii of each circle. We repeated this for 25 pairs of images that were identical except for photon shot noise and used the root-mean-square error of protein height as an error (*SI Appendix*, Table S1).

Effect of Vibrations on CSOP Height Measurements. To simulate acoustic vibration (*SI Appendix*, Fig. S9), we allowed a circle as described in the previous section to move five steps in a random orientation and accumulated images of circles in five different positions to make one image frame.

MD Simulation Overview. To explore a molecular model of protein dynamics on fluid membranes, we performed coarse-grained MD simulations of semiflexible polymers diffusing on 2D surfaces. We model protein chains using a standard Kremer–Grest bead–spring model (57), with each bead representing a structured protein domain (*SI Appendix*, Fig. S4). Simulations were performed using a graphics processing unit (GPU)-enabled HOOMD-blue MD package (58, 59), and all simulation results constitute an average of over at least 2,000 protein chains. All bead pair interactions and bead–wall interactions are modeled with a Weeks–Chandler–Andersen potential (60). All lengths are expressed in units of the Lennard-Jones (LJ) diameter σ and are set to unity. We connect the polymer chains with a finitely extensible nonlinear elastic potential, using a spring constant of $k = 30$ and a bond length of $R_0 = 1.5$ (expressed in terms of reduced LJ units $\epsilon = \sigma = 1$). We used a system box size of $V = L^2L_z$ with $L_z = 50\sigma$, and L was adjusted to achieve the specified area density and number of polymer chains (*SI Appendix*, Fig. S4). Dilute surface densities were conducted with ∼200 chains per square micrometer, and the dense surfaces went up to ∼20,000 chains per square micrometer. We imposed periodic boundary conditions in all directions, although the direction tangential to the substrate does not require them, because the bottom wall prevents any particles from passing through. Initial configurations are generated by placing the particles in lattice locations, and sufficient time steps are run to reach a steady state. Time steps were varied from $\Delta t = 10^{-6}$ to 10^{-4} and verified to be sufficiently small to capture relevant dynamics.

To model semiflexible polymers, we implemented a bending potential between three neighboring particles to capture chain stiffness, $U_B = \epsilon_B(1 - \cos(\theta_{ijk} - \theta_0))$, where ϵ_B is the bending energy, θ_{ijk} is the bond angle between neighboring particles (i, j, k), and $\theta_0 = \pi$ is the resting angle (*SI Appendix*, Fig. S4 and Movie S1).

For simulations of macromolecular osmotic compression, spherical particles were added to the bulk of the simulation box to model the effects of macromolecular crowding. To model PEG8k used in the experiments, these bulk particles were chosen to have a soft repulsive potential between particle pairs. The radius of gyration of PEG8k was estimated to be within the range of 2.5 nm to 3.4 nm (61–63), which forms the upper and lower bounds of simulation data (Fig. 2*E* and Movie S2).

For simulations of antibody labeling of cell surface proteins, we constructed an antibody using a rigid assembly of five spheres using physical dimensions of IgG antibodies: ∼15 nm wide, ∼8 nm tall, and ∼4 nm thick (64, 65) (*SI Appendix*, Fig. S8 and Movie S3). We assign one of the Fab domains to bind strongly to a single domain on the protein chain. The attractive pair potential between these two particles is radially symmetric such that the antibody can swing freely in all angles around the protein binding site. We calculate the average offset of the center of mass of the antibody relative to the binding site on the protein. Although it is known that antibodies are flexible macromolecules (65, 66), we modeled them as a rigid assembly, for simplicity (see *SI Appendix* for MD simulation details).

Data Availability. The CSOP measurement protocols are described in *Materials and Methods* and *SI Appendix, SI Text*. The sequence of size standard DNAs and the coding sequence of recombinant proteins are available in *SI Appendix*. The antibodies are described in *SI Appendix*. Custom Matlab scripts for processing and simulating CSOP images are available in ref. 56.

ACKNOWLEDGMENTS. We would like to thank the D.A.F. laboratory members for feedback. We thank Dr. Erik Voets and Aduro Biotech for supplying the anti-SIRPα antibody. The illustration of proteins in Fig. 2*C* is made using cellscape by Jordi Silvestre-Ryan (https://github.com/jordisr/cellscape). This work was supported by NIH Grant R01 GM114671 (D.A.F.), the Immunotherapeutics and Vaccine Research Initiative at University of California, Berkeley (D.A.F.), the Miller Institute for Basic Research, and the Chan Zuckerberg Biohub (D.A.F.). S.S. was funded by a Life Science Research Foundation fellowship. B.B. was supported by the NIH Ruth L. Kirschstein NIH National Research Service Award fellowship (Grant 1F32GM115091). S.C.T. acknowledges support from the Miller Institute for Basic Research in Science at University of California, Berkeley. D.A.F. is a Chan Zuckerberg Biohub investigator.

1. D. Hatherley *et al*., Paired receptor specificity explained by structures of signal regulatory proteins alone and complexed with CD47. *Mol. Cell* **31**, 266–277 (2008).
2. D. Bausch-Fluck *et al*., The in silico human surfaceome. *Proc. Natl. Acad. Sci. U.S.A.* **115**, E10988–E10997 (2018).
3. D. N. Itzhak, S. Tyanova, J. Cox, G. H. Borner, Global, quantitative and dynamic mapping of protein subcellular localization. *eLife* **5**, e16950 (2016).
4. P. Anton van der Merwe, S. J. Davis, A. S. Shaw, M. L. Dustin, Cytoskeletal polarization and redistribution of cell-surface molecules during T cell antigen recognition. *Semin. Immunol.* **12**, 5–21 (2000).
5. K. Choudhuri, D. Wiseman, M. H. Brown, K. Gould, P. A. van der Merwe, T-cell receptor triggering is critically dependent on the dimensions of its peptide-MHC ligand. *Nature* **436**, 578–582 (2005).
6. S.-P. Cordoba *et al*., The large ectodomains of CD45 and CD148 regulate their segregation from and inhibition of ligated T-cell receptor. *Blood* **121**, 4295–4302 (2013).
7. J. R. James, R. D. Vale, Biophysical mechanism of T-cell receptor triggering in a reconstituted system. *Nature* **487**, 64–69 (2012).
8. J. H. Felce *et al*., CD45 exclusion– and cross-linking–based receptor signaling together broaden FcεRI reactivity. *Sci. Signal.* **11**, eaat0756 (2018).
9. M. H. Bakalar *et al*., Size-dependent segregation controls macrophage phagocytosis of antibody-opsonized targets. *Cell* **174**, 131–142.e13 (2018).
10. M. J. Paszek *et al*., The cancer glycocalyx mechanically primes integrin-mediated growth and survival. *Nature* **511**, 319–325 (2014).
11. E. C. Woods *et al*., A bulky glycocalyx fosters metastasis formation by promoting G1 cell cycle progression. *eLife* **6**, e25752 (2017).
12. M. J. Paszek, D. Boettiger, V. M. Weaver, D. A. Hammer, Integrin clustering is driven by mechanical resistance from the glycocalyx and the substrate. *PLoS Comput. Biol.* **5**, e1000604 (2009).
13. J. Hu, R. Lipowsky, T. R. Weikl, Binding constants of membrane-anchored receptors and ligands depend strongly on the nanoscale roughness of membranes. *Proc. Natl. Acad. Sci. U.S.A.* **110**, 15283–15288 (2013).
14. J. Hegermann, H. Lünsdorf, M. Ochs, H. Haller, Visualization of the glomerular endothelial glycocalyx by electron microscopy using cationic colloidal thorium dioxide. *Histochem. Cell Biol.* **145**, 41–51 (2016).
15. E. E. Ebong, F. P. Macaluso, D. C. Spray, J. M. Tarbell, Imaging the endothelial glycocalyx in vitro by rapid freezing/freeze substitution transmission electron microscopy. *Arterioscler. Thromb. Vasc. Biol.* **31**, 1908–1915 (2011).
16. M. J. Paszek *et al*., Scanning angle interference microscopy reveals cell dynamics at the nanoscale. *Nat. Methods* **9**, 825–827 (2012).
17. V. Kiessling, L. K. Tamm, Measuring distances in supported bilayers by fluorescence interference-contrast microscopy: Polymer supports and SNARE proteins. *Biophys. J.* **84**, 408–418 (2003).
18. R. Parthasarathy, J. T. Groves, Protein patterns at lipid bilayer junctions. *Proc. Natl. Acad. Sci. U.S.A.* **101**, 12798–12803 (2004).
19. R. Roy, S. Hohng, T. Ha, A practical guide to single-molecule FRET. *Nat. Methods* **5**, 507–516 (2008).
20. G. Shtengel *et al*., Interferometric fluorescent super-resolution microscopy resolves 3D cellular ultrastructure. *Proc. Natl. Acad. Sci. U.S.A.* **106**, 3125–3130 (2009).
21. B. Huang, W. Wang, M. Bates, X. Zhuang, Three-dimensional super-resolution imaging by stochastic optical reconstruction microscopy. *Science* **319**, 810–813 (2008).
22. M. F. Juette *et al*., Three-dimensional sub-100 nm resolution fluorescence microscopy of thick samples. *Nat. Methods* **5**, 527–529 (2008).
23. S. Abrahamsson *et al*., Fast multicolor 3D imaging using aberration-corrected multifocus microscopy. *Nat. Methods* **10**, 60–63 (2013).
24. P. Kanchanawong *et al*., Nanoscale architecture of integrin-based cell adhesions. *Nature* **468**, 580–584 (2010).
25. C. Bertocchi *et al*., Nanoscale architecture of cadherin-based cell adhesions. *Nat. Cell Biol.* **19**, 28–37 (2017).
26. L. Möckl *et al*., Quantitative super-resolution microscopy of the mammalian glycocalyx. *Dev. Cell* **50**, 57–72.e6 (2019).
27. A. Pertsinidis, Y. Zhang, S. Chu, Subnanometre single-molecule localization, registration and distance measurements. *Nature* **466**, 647–651 (2010).
28. F. Balzarotti *et al*., Nanometer resolution imaging and tracking of fluorescent molecules with minimal photon fluxes. *Science* **355**, 606–612 (2017).
29. R. E. Thompson, D. R. Larson, W. W. Webb, Precise nanometer localization analysis for individual fluorescent probes. *Biophys. J.* **82**, 2775–2783 (2002).
30. B. Huang, H. Babcock, X. Zhuang, Breaking the diffraction barrier: Super-resolution imaging of cells. *Cell* **143**, 1047–1058 (2010).
31. M. J. Rust, M. Bates, X. Zhuang, Sub-diffraction-limit imaging by stochastic optical reconstruction microscopy (STORM). *Nat. Methods* **3**, 793–795 (2006).
32. S. Niekamp *et al*., Nanometer-accuracy distance measurements between fluorophores at the single-molecule level. *Proc. Natl. Acad. Sci. U.S.A.* **116**, 4275–4284 (2019).
33. M. D. Lew, M. P. Backlund, W. E. Moerner, Rotational mobility of single molecules affects localization accuracy in super-resolution fluorescence microscopy. *Nano Lett.* **13**, 3967–3972 (2013).
34. C. G. Baumann, S. B. Smith, V. A. Bloomfield, C. Bustamante, Ionic effects on the elasticity of single DNA molecules. *Proc. Natl. Acad. Sci. U.S.A.* **94**, 6185–6190 (1997).
35. B. A. Cornell, F. Separovic, Membrane thickness and acyl chain length. *Biochim. Biophys. Acta* **733**, 189–193 (1983).
36. J. C. Stachowiak *et al*., Membrane bending by protein-protein crowding. *Nat. Cell Biol.* **14**, 944–949 (2012).
37. T. Peters Jr., *All About Albumin: Biochemistry, Genetics, and Medical Applications*, (Academic, 1995).
38. B. Button *et al*., A periciliary brush promotes the lung health by separating the mucus layer from airway epithelia. *Science* **337**, 937–941 (2012).
39. E. M. J. Siren, R. Chapanian, I. Constantinescu, D. E. Brooks, J. N. Kizhakkedathu, Oncotically driven control over glycocalyx dimension for cell surface engineering and protein binding in the longitudinal direction. *Sci. Rep.* **8**, 7581 (2018).
40. W. M. Abbott, M. M. Damschroder, D. C. Lowe, Current approaches to fine mapping of antigen-antibody interactions. *Immunology* **142**, 526–535 (2014).
41. C. B. Carbone *et al*., In vitro reconstitution of T cell receptor-mediated segregation of the CD45 phosphatase. *Proc. Natl. Acad. Sci. U.S.A.* **114**, E9338–E9345 (2017).
42. V. T. Chang *et al*., Initiation of T cell signaling by CD45 segregation at "close contacts.". *Nat. Immunol.* **17**, 574–582 (2016).
43. V. Junghans *et al*., Hydrodynamic trapping measures the interaction between membrane-associated molecules. *Sci. Rep.* **8**, 12479 (2018).
44. A. Varki *et al*., *Essentials of Glycobiology*, (Cold Spring Harbor Laboratory Press, ed. 2, 2009).
45. E. Sezgin *et al*., Elucidating membrane structure and protein behavior using giant plasma membrane vesicles. *Nat. Protoc.* **7**, 1042–1051 (2012).
46. C. King, M. Stoneman, V. Raicu, K. Hristova, Fully quantified spectral imaging reveals in vivo membrane protein interactions. *Integr. Biol.* **8**, 216–229 (2016).
47. A. D. Skinkle, K. R. Levental, I. Levental, Cell-derived plasma membrane vesicles are permeable to hydrophilic macromolecules. *Biophys. J.* **118**, 1292–1300 (2020).
48. D. Virant *et al*., A peptide tag-specific nanobody enables high-quality labeling for dSTORM imaging. *Nat. Commun.* **9**, 930 (2018).
49. F. Lang *et al*., Functional significance of cell volume regulatory mechanisms. *Physiol. Rev.* **78**, 247–306 (1998).
50. G. G. Wang *et al*., Quantitative production of macrophages or neutrophils ex vivo using conditional Hoxb8. *Nat. Methods* **3**, 287–293 (2006).
51. C. B. Rosen, M. B. Francis, Targeting the N terminus for site-selective protein modification. *Nat. Chem. Biol.* **13**, 697–705 (2017).
52. M. L. Hermiston, Z. Xu, A. Weiss, CD45: A critical regulator of signaling thresholds in immune cells. *Annu. Rev. Immunol.* **21**, 107–137 (2003).
53. D. K. Das *et al*., Direct visualization of the conformational dynamics of single influenza hemagglutinin trimers. *Cell* **174**, 926–937.e12 (2018).
54. J. Yin *et al*., Genetically encoded short peptide tag for versatile protein labeling by Sfp phosphopantetheinyl transferase. *Proc. Natl. Acad. Sci. U.S.A.* **102**, 15815–15820 (2005).
55. C. S. Theile *et al*., Site-specific N-terminal labeling of proteins using sortase-mediated reactions. *Nat. Protoc.* **8**, 1800–1807 (2013).
56. S. Son *et al*, Supplementary software - Molecular height measurement by cell surface optical profilometry (CSOP). Github. https://github.com/smson-ucb/CSOP. Deposited 30 May 2020.

57. K. Kremer, G. S. Grest, Dynamics of entangled linear polymer melts: A molecular-dynamics simulation. *J. Chem. Phys.* **92**, 5057–5086 (1990).
58. J. A. Anderson, C. D. Lorenz, A. Travesset, General purpose molecular dynamics simulations fully implemented on graphics processing units. *J. Comput. Phys.* **227**, 5342–5359 (2008).
59. J. Glaser *et al*., Strong scaling of general-purpose molecular dynamics simulations on GPUs. *Comput. Phys. Commun.* **192**, 97–107 (2015).
60. J. D. Weeks, D. Chandler, H. C. Andersen, Role of repulsive forces in determining the equilibrium structure of simple liquids. *J. Chem. Phys.* **54**, 5237–5247 (1971).
61. K. Devanand, J. C. Selser, Asymptotic behavior and long-range interactions in aqueous solutions of poly(ethylene oxide). *Macromolecules* **24**, 5943–5947 (1991).
62. K. A. Rubinson, S. Krueger, Poly(ethylene glycol)s 2000–8000 in water may be planar: A small-angle neutron scattering (SANS) structure study. *Polymer (Guildf.)* **50**, 4852–4858 (2009).
63. K. L. Linegar, A. E. Adeniran, A. F. Kostko, M. A. Anisimov, Hydrodynamic radius of polyethylene glycol in solution obtained by dynamic light scattering. *Colloid J.* **72**, 279–281 (2010).
64. Y. H. Tan *et al*., A nanoengineering approach for investigation and regulation of protein immobilization. *ACS Nano* **2**, 2374–2384 (2008).
65. C. De Michele, P. De Los Rios, G. Foffi, F. Piazza, Simulation and theory of antibody binding to crowded antigen-covered surfaces. *PLoS Comput. Biol.* **12**, e1004752 (2016).
66. L. Bongini *et al*., Freezing immunoglobulins to see them move. *Proc. Natl. Acad. Sci. U.S.A.* **101**, 6466–6471 (2004).